Connexin 43 connexon to gap junction transition is regulated by zonula occludens-1

J. Matthew Rhett, Jane Jourdan, and Robert G. Gourdie
Department of Regenerative Medicine and Cell Biology, Medical University of South Carolina, Charleston, SC 29425

ABSTRACT Connexin 43 (Cx43) is a gap junction (GJ) protein widely expressed in mammalian tissues that mediates cell-to-cell coupling. Intercellular channels comprising GJ aggregates form from docking of paired connexons, with one each contributed by apposing cells. Zonula occludens-1 (ZO-1) binds the carboxy terminus of Cx43, and we have previously shown that inhibition of the Cx43/ZO-1 interaction increases GJ size by 48 h. Here we demonstrated that increases in GJ aggregation occur within 2 h (~Cx43 half-life) following disruption of Cx43/ZO-1. Immunoprecipitation and Duolink protein–protein interaction assays indicated that inhibition targets ZO-1 binding with Cx43 in GJs as well as connexons in an adjacent domain that we term the "perinexus." Consistent with GJ size increases being matched by decreases in connexons, inhibition of Cx43/ZO-1 reduced the extent of perinexal interaction, increased the proportion of connexons docked in GJs relative to undocked connexons in the plasma membrane, and increased GJ intercellular communication while concomitantly decreasing hemichannel-mediated membrane permeance in contacting, but not noncontacting, cells. ZO-1 small interfering RNA and overexpression experiments verified that loss and gain of ZO-1 function govern the transition of connexons into GJs. It is concluded that ZO-1 regulates the rate of undocked connexon aggregation into GJs, enabling dynamic partitioning of Cx43 channel function between junctional and proximal nonjunctional domains of plasma membrane.

INTRODUCTION

Gap junctions (GJs) consist of a lattice of intercellular channels enabling the diffusion of small molecules (<1000 Da) between cells. Intercellular channels are composed of two hexameric oligomers called connexons or hemichannels, with one each contributed by contacting cells (Koval, 2006; Laird, 2006). The GJ protein connexin 43 (Cx43) is the most ubiquitous connexin, with expression in at least 46 different cell types (Solan and Lampe, 2009), most notably in the heart (van Veen et al., 2001; Desplantez et al., 2007; Severs et al., 2008; Noorman et al., 2009) and skin (Guo et al., 1992; Goliger and Paul, 1995; Coutinho et al., 2003; Kretz et al., 2004). In the mammalian heart Cx43 is the primary connexin expressed in the working ventricular myocardium, where it preferentially localizes to the intercalated disk (ID), and is thought to be responsible for propagation of the action potential (Miquerol et al., 2003; Severs et al., 2008).

Regulation of GJ coupling is a necessary component of cellular function and response to physiological and pathological stimuli. Under pathological conditions in the heart, Cx43 expression and subcellular localization are dysregulated in a process called GJ remodeling (Desplantez et al., 2007). Decreases in Cx43 expression are documented for nearly every type of cardiac pathology, and during the acute phase of ischemia in a myocardial infarction Cx43 is redistributed to the sides of cardiomyocytes in a process called lateralization, with potentially arrhythmogenic consequences (Smith et al., 1991; Matsushita et al., 1999; Severs et al., 2008).

Cells modify the expression, phosphorylation state, and protein interactions of Cx43 throughout the cell cycle (Solan et al., 2003; Doble et al., 2004; Singh et al., 2005). Because of the short half-life of

Cx43, which is as little as 1–2 h (Laird et al., 1991), regulation appears to exist on both short and long time scales through phosphorylation and protein interaction, and gene expression, respectively. Currently, there is a great deal of data on phospho- and transcriptional regulation of Cx43 (Lampe and Lau, 2004; Oyamada et al., 2005; Solan and Lampe, 2009), but less is known about the mechanistic basis and function of Cx43 protein–protein interactions (Giepmans, 2004).

The addition and removal of intercellular channels to and from GJs provide a direct means of controlling the level of GJ intercellular communication (GJIC) between cells. It has been shown that new connexons are added to GJs at the periphery of the aggregate (Gaietta et al., 2002). The scaffold protein zonula occludens-1 (ZO-1) has been shown to interact with the carboxy terminus (CT) of Cx43 (Giepmans and Moolenaar, 1998; Toyofuku et al., 1998), and work performed in our laboratory and others has shown that the Cx43/ZO-1 interaction is involved in GJ size regulation (Hunter et al., 2003, 2005; Maass et al., 2007). Specifically, it was demonstrated that reduction (Hunter et al., 2005) or prohibition (Hunter et al., 2003, 2005; Maass et al., 2007) of the Cx43/ZO-1 interaction resulted in increased GJ size and a decrease or loss of colocalization between Cx43 and ZO-1 at plaque edges, respectively. Interestingly, it has been recently found that the interaction of Cx43 and ZO-1 is increased in the IDs of ventricular cardiomyocytes from heart failure patients (Bruce et al., 2008).

On the basis of these studies, we hypothesized that ZO-1 dynamically regulates the accretion of Cx43 GJ intercellular channels from cell-surface pools of unaggregated connexons. It has been established that undocked connexons in the plasma membrane can and do open in response to various treatments and (patho)physiological stimuli (Saez et al., 2003). In particular, cardiomyocyte Cx43 hemichannels have been shown to open in response to metabolic inhibition and ischemia resulting in cell death and ATP release, possibly exerting a proarrhythmogenic response (John et al., 1999; Shintani-Ishida et al., 2007; Clarke et al., 2009).

Herein we provide evidence that ZO-1 regulates the transition of undocked connexons into GJs from novel domains of proximal membrane. In addition, we show that changes in the Cx43/ZO-1 interaction affecting this transition have complementary effects on GJIC and connexon function. Our results indicate that the level of ZO-1/Cx43 interaction inversely determines a balance between the dual role of the connexon in GJIC and hemichannel function in a localized manner at GJs.

RESULTS

ZO-1 regulates connexon recruitment from a novel region proximal to the GJ

GJ size, as measured by confocal immunofluorescence, is a well-established metric for GJ aggregation (Gourdie et al., 1991; Green et al., 1993; Kaprielian et al., 1998; Hunter et al., 2005). We have previously shown that the Cx43 CT mimetic peptide, αCT-1, efficiently enters the cytoplasm, binds to the second postsynaptic density 95/disc-large/zona occludens (PDZ2) domain of ZO-1, and competitively inhibits the interaction of endogenous Cx43 with ZO-1 (Hunter et al., 2005). Furthermore, this disruption of the Cx43/ZO-1 interaction results in larger GJ plaques (Hunter et al., 2005).

Here we have attempted to further define the interaction mechanistically and in terms of spatial and temporal resolution. Specifically, temporal resolution was addressed by studying the interaction on a 2 h time scale, in line with the half-life of Cx43 (Laird et al., 1991; Laird, 1996; Darrow et al., 1995; Saffitz et al., 2000; Hunter et al., 2005), and we gained further insight into the mechanism by examining how actin, a known binding partner of ZO-1

(Gonzalez-Mariscal et al., 2000), codistributed with GJs and immunoprecipitated with ZO-1. Finally, spatial resolution was achieved using the novel Duolink assay, which allowed an in situ examination of the protein–protein interaction between Cx43 and ZO-1.

It was found that cells treated with αCT-1 for 2 h displayed larger cell border–localized GJs than either vehicle or reverse control peptide–treated control groups (Figure 1A). Quantification of GJ size confirmed that the observed changes were significantly different (Figure 1C) and at a similar level to our previously published results conducted on a longer, 48 h time scale (Hunter et al., 2005).

Cx43-expressing HeLa (Cx43-HeLa) cells were transfected with a plasmid expressing ZO-1 in order to increase Cx43/ZO-1 interaction, as confirmed by colocalization analysis (Figure 1E). Transfection efficiency by the DsRed-tagged full-length ZO-1 construct was low, but conveniently this facilitated a direct comparison of GJ size between nearby untransfected and transfected cells within the monolayer. Visual inspection of immunolabeled optical sections indicated that ZO-1–overexpressing cells generated smaller GJs, with higher levels of colocalized ZO-1, than adjacent control sister cells (Figure 1, B and E). GJ size was quantified and found to be smaller in ZO-1–overexpressing cells (Figure 1D). It was concluded that loss or gain of ZO-1 association was consistent with increased and reduced connexon aggregation into GJs, respectively.

To gain insight into the mechanism of ZO-1–regulated GJ accretion, immunoprecipitation of ZO-1 from fractionated Cx43-HeLa cell lysates was performed. Cx43-HeLa cell lysates were fractionated based on Triton X-100 solubility to separate GJ Cx43 from nonjunctional Cx43 (Musil and Goodenough, 1991; Hunter et al., 2005). ZO-1 was then immunoprecipitated from these fractions followed by Western blot against Cx43 and actin, another known binding partner of ZO-1 (Gonzalez-Mariscal et al., 2000). It was found that Cx43 coimmunoprecipitated with ZO-1 in both nonjunctional (Triton-soluble) and junctional (Triton-insoluble) fractions (Figure 1F), indicating that ZO-1 interacts with both connexons and GJ intercellular channels. Interestingly, actin coimmunoprecipitated with ZO-1 only in the Triton-insoluble fraction (Figure 1F). This suggested that ZO-1, actin, and Cx43 were present in the same multiprotein complex only when connexons were aggregated in detergent-resistant GJs.

Subcellular localization of the Cx43/ZO-1 interaction was visualized using a Duolink assay for Cx43/ZO-1 interaction in situ. This assay works similarly to standard immunofluorescence detection, except that the secondary antibodies are conjugated to oligonucleotides that comprise one-half of a closed circle that can be ligated together only when the antibodies are in close proximity (<40 nm; Gullberg, 2010). This complex can then be detected by rolling circle amplification of the closed circle and addition of a complementary, fluorescently tagged oligonucleotide. For our purposes primary antibodies against Cx43 and ZO-1 were used for Duolink detection of the Cx43/ZO-1 interaction, while a separate primary antibody was used to detect Cx43. This was applied to the same cultures already described in Figure 1A. In this way, the site of the Cx43/ZO-1 interaction relative to Cx43 GJs and the actin cytoskeleton could be visualized. Under control conditions, it was found that the Cx43/ZO-1 interaction occurred throughout cells, and primarily at cell–cell borders (Figure 2A). Moreover, Duolink fluorescence was observed to cluster at GJs. Expanded views of regions containing GJs revealed that some of the clustered Duolink fluorescence overlapped with GJs, with the bulk of the signal typically located in the region proximally adjacent to GJs (Figure 2A).

Interestingly, while the Cx43/ZO-1 interaction that took place within GJs frequently overlapped with actin staining (arrowheads,
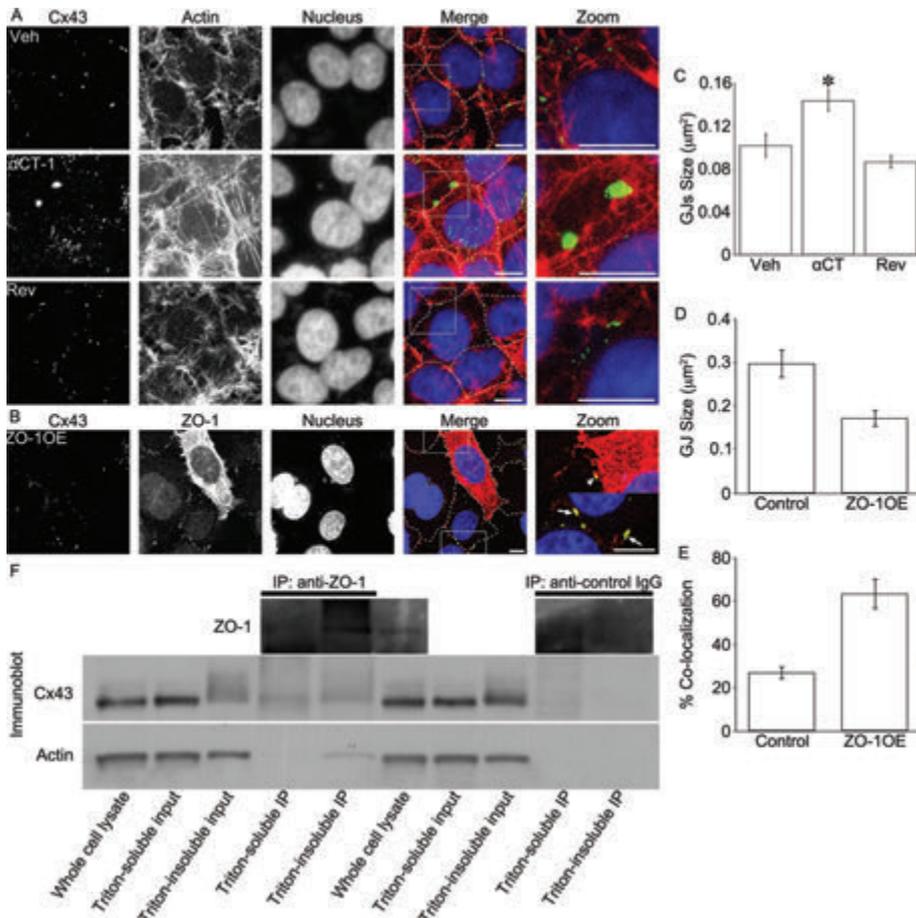
FIGURE 1: ZO-1 regulates GJ accretion. (A) Representative confocal images of Cx43-HeLa cells treated with either vehicle (Veh), αCT-1, or reverse control peptide (Rev) for 2 h followed by fixation and labeling for the nucleus (blue), cytoskeleton (red), and Cx43 (green). These representative images are maximum projections of Z stacks from three separate experiments in which 15 optical fields were imaged. Cell borders are indicated by dashed lines. (B) Confocal immunofluorescent images of ZO-1–overexpressing (ZO-1OE) HeLa cells stained for the nucleus (blue), ZO-1 (red), and Cx43 (green). ZO-1OE cells are clearly distinguishable from sister cells by bright red staining. Arrows indicate examples of Cx43 GJ staining, and arrowheads highlight visible GJs in ZO-1OE cells. This representative image is from 10 optical fields taken from a single experiment. The rightmost panels in (A) and (B) are expanded views of the boxed regions in the adjacent panels to the left. (C) Quantification of GJ area from confocal images of vehicle (Veh)–, αCT-1–, and reverse control peptide (Rev)–treated cells shows that disruption of the Cx43/ZO-1 interaction acutely and significantly increases GJ size. *P < 0.05 vs. all other groups; N = 3. (D) Quantification of GJ area from confocal images of ZO-1OE cells shows that ZO-1OE decreases GJ size in comparison to "control" sister cells. GJ size was determined in control and ZO-1OE cells within the same image. (E) Quantification of Cx43 colocalized with ZO-1 showed increased superposition of Cx43 and ZO-1 signal in ZO-1OE cells. (F) Representative blots of ZO-1 (top), Cx43 (middle), and actin (bottom) immunoprecipitated with ZO-1 or control IgG. Scale bars = 10 μm.

αCT-1, which correlates to an increase in GJ size.

Similar results demonstrating a region enriched for Cx43/ZO-1 interaction adjacent to GJs were obtained with rat epicardial cells (RECs). RECs displayed a pattern of staining similar to that found in Cx43-HeLa cells (compare controls in Figure 2, A and B), with the exception that, overall, more Duolink fluorescence was observed. From these images it was clear that the extent of GJ-associated Duolink fluorescence (white dashed line, Figure 2B) well exceeded the perimeter of the GJ (black dotted line, Figure 2B). The space around GJs containing Cx43 connexons interacting with ZO-1 represents a heretofore unrecognized region of specialization in the membrane that we have termed the *perinexus*.

Connexon accretion to GJs is controlled by ZO-1 binding of the Cx43 CT

The above results in combination with the canonical GJ-perimeter pathway for addition of new connexons to the plaque (Gaietta *et al.*, 2002) suggested that ZO-1 regulated the rate of GJ accretion from plasma membrane connexons. This hypothesis was tested by a pulse-chase, cell-surface protein biotinylation assay. Here an approach modified from the method of Musil and Goodenough was used (Musil and Goodenough, 1991; VanSlyke and Musil, 2005). Briefly, biotin was pulsed on cells for 15 min followed by a 2 h chase period, during which time the cells were exposed to αCT-1 or controls. The purpose here was to determine whether inhibiting Cx43/ZO-1 increased the shift of cell-surface Cx43 from nonjunctional to junctional pools (Figure 3A).

Control cells that were returned to culture conditions during the chase period displayed an increase in the relative amount of biotin-tagged, Triton X-100–insoluble Cx43 (Figure 3). This indicates accretion of undocked connexons in the membrane into GJs that is ongoing over the 2 h time course—a pattern consistent with previous reports (Musil and Goodenough, 1991). However, in a novel result, if cells were returned to incubation for 2 h in the presence of αCT-1, the ratio of detergent-insoluble to detergent-soluble Cx43 increased significantly above that found in control conditions after 2 h (Figure 3B).

These data are consistent with a mechanism in which Cx43 GJs accrete from a cell-surface connexon pool of Cx43 and that presence of high levels of the Cx43 PDZ-binding ligand (αCT-1) in the cell cytoplasm enhances the rate of recruitment from that same pool of connexons. This may be attributed to increased binding of the ZO-1 PDZ2 domain by αCT-1, resulting in a shift within the cell-surface pool of Cx43 in which the proportion of connexons docked within GJs increased relative to undocked connexons free in the

Figure 2A), Duolink fluorescence adjacent to GJs typically did not overlap with the actin cytoskeleton (arrows, Figure 2A). Conversely, αCT-1–treated cultures displayed far less Duolink fluorescence at and around GJs (Figure 2, A and C). In accordance with these observations, low-intensity Cx43 staining was observed encircling junctions when the gain was increased, indicating a higher concentration of Cx43 channels in this region as compared with other areas in the plasma membrane not associated with GJs. In combination with the immunoprecipitation data, these results indicate that the Cx43/ZO-1 interaction localizes to both intercellular channels within GJs and connexons proximal to GJ plaques. Furthermore, this pattern of interaction can be disrupted by
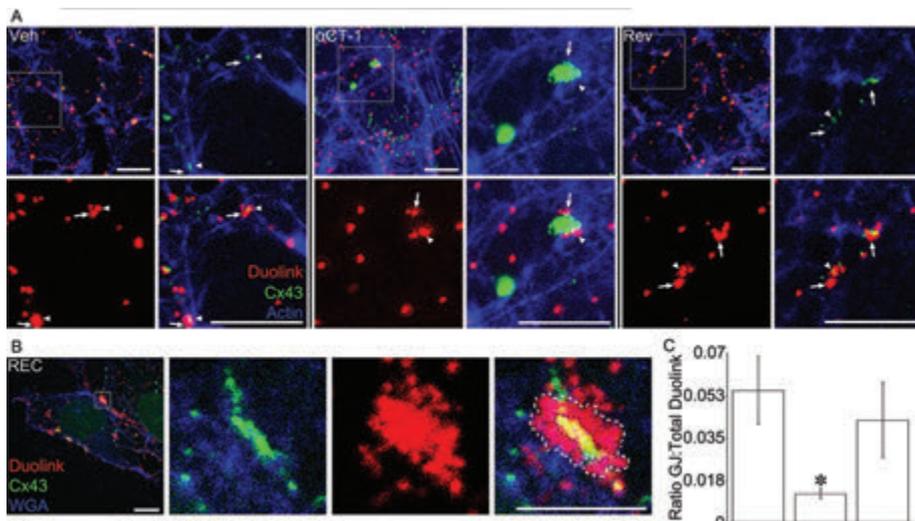
FIGURE 2: ZO-1 interacts with Cx43 in the perinexus. (A) Representative confocal images of the same fields in Figure 1A, omitting nuclear fluorescence and adding Duolink fluorescence (Cx43/ZO-1 interaction; red). Actin is labeled in blue, and Cx43 is labeled in green. Vehicle (Veh), αCT-1, and reverse control peptide (Rev) are shown on the left, center, and right, respectively. For each treatment an expanded view of the boxed region in the top left panel is given in the other three panels, which show Cx43 plus actin staining (top right), Duolink alone (bottom left), and merged images (bottom right). Arrows indicate Duolink fluorescence that is adjacent to GJs but does not appear to overlap with actin. Arrowheads indicate Duolink spots that overlap with Cx43 and, frequently, actin fluorescence. (B) Representative confocal image of RECs expressing Cx43-EGFP (green) and labeled for plasma membrane (WGA; blue) and Duolink fluorescence (Cx43/ZO-1 interaction; red). The boxed region of the leftmost image is expanded in the other three panels, showing (from left to right) Cx43 plus plasma membrane fluorescence, Duolink fluorescence, and a merged image. In the rightmost panel, the dashed white line indicates the extent of Duolink stain, and the dotted black line indicates the perimeter of the GJ. We have termed the intervening perijunctional space the perinexus. (C) An analysis of the staining pattern of Duolink fluorescence colocalized with Cx43 fluorescence in the experiment represented in (A). The ratio of Duolink fluorescence overlapping with Cx43 fluorescence to total Duolink fluorescence was significantly reduced in αCT-1 as compared with vehicle. *P < 0.05 vs. Veh; N = 3. The scale bars = 10 μm except for the enlarged images in (B), which equal 5 μM. Error bars represent the standard error of the mean (SEM) for all panels.

plasma membrane. The reduction in perinexal Cx43/ZO-1 interaction associated with αCT-1 treatment indicated in Figure 2A suggests that the majority of connexons in the biotinylation assay were recruited from pools proximal to the GJ—that is, from the perinexus.

Disruption of the Cx43/ZO-1 interaction increases GJIC

We hypothesized that a consequence of the increased GJ aggregation observed by confocal microscopy and biotin tagging of connexons following targeting of the ZO-1/Cx43 interaction would be increased levels of GJIC. To determine whether this was the case, experiments investigating GJIC were carried out using a simple neurobiotin scrape-loading assay.

In these GJIC experiments, it was found that wild-type HeLa cells, not expressing Cx43, displayed neurobiotin uptake only in injured cells at the edge of a scraped monolayer and did not transfer neurobiotin to uninjured, adjacent cells (Figure 4A). Therefore these cells appeared not to communicate via GJs at detectable levels.

By contrast, vehicle and reverse control–treated injured Cx43-HeLa cells showed dye diffusion to adjacent cells several layers from the edge of the scratch, and cells treated with αCT-1 displayed an even greater distance of dye spread (Figure 4A). Quantification of

the distance of dye spread confirmed that Cx43-HeLa cells transferred dye to a significantly greater distance than wild-type HeLa cells and that αCT-1–treated Cx43-HeLa cells displayed significantly greater communication than control Cx43-HeLa cells (Figure 4B). On the basis of these data, we concluded that Cx43 GJs mediated dye spread in this assay and that disruption of the Cx43/ZO-1 interaction increased GJIC.

Cell injury (e.g., as occurs during scrape loading) may affect channel gating (Richards et al., 2004). Therefore gap fluorescence recovery after photobleaching (gap-FRAP) was used as an alternative approach for evaluation of GJIC. Consistent with the literature, we found that individual bleached Cx43-expressing cells recovered fluorescence following cessation of a brief pulse of high-intensity laser illumination, while those treated with heptanol or not expressing connexin did not recover (Figure 5, A and B) (Bastide et al., 1995; Abbaci et al., 2007, 2008).

Reverse control peptide–treated cells recovered similarly to vehicle, while αCT-1– treated cells recovered much more rapidly than either of the two control groups (Figure 5, A and B). To test the possibility that the effects of αCT-1 were due to affects on channel gating, αCT-1 cultures were also treated with heptanol. Cells treated with heptanol + αCT-1 did not recover faster than either Cx43-HeLa cells treated with heptanol alone or wild-type HeLa cells (Figure 5, A and B).

A quantitative assessment of GJIC, assayed by FRAP, was carried out by linear regression of fluorescence recovery values to an exponential decay function commonly used for analysis of gap-FRAP experiments (Salmon et al., 1984; Abbaci et al., 2007, 2008). αCT-1–treated Cx43-HeLa cells had a slightly greater, but not statistically different, value for maximal recovery, F_∞, than controls (Figure 5C). This indicated that recovery was predicted to occur to a similar level in vehicle, αCT-1, and reverse control peptide–treated groups. Importantly, however, αCT-1–treated cells recovered fluorescence significantly faster than the controls, as assessed from the rate constant, k (Figure 5D). These data corroborate the scrape-loading results, showing that αCT-1 expedited the rate of recovery by increasing GJIC.

Taken together, our results indicate that disruption of the Cx43/ZO-1 interaction by targeting the ZO-1 PDZ2 domain increased GJIC over short time scales. We posit that the increased recruitment of connexons from free perinexal membrane pools into GJs observed by immunofluorescence, Duolink, and biotin-tagging assays was concomitant with an increase in GJIC.

As a further approach to reducing the Cx43/ZO-1 interaction, small interfering RNA (siRNA) was used to knock down ZO-1 levels. Western blotting demonstrated that transient transfection of ZO-1 siRNA reduced ZO-1 levels to <60% of untransfected controls, while Cx43 levels were unaffected (Figure 6, A–C). Although higher levels of ZO-1 knockdown could be achieved (Supplemental Figure 2), this midrange knockdown was used intentionally to avoid pleiotropic
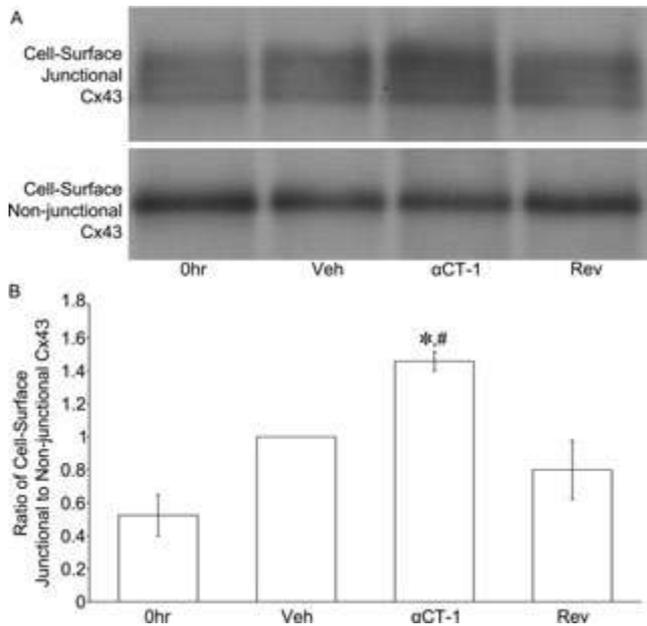
FIGURE 3: The proportion of Cx43 hemichannels contributing to GJ accretion is increased by Cx43/ZO-1 disengagement. (A) Representative blot of Triton X-100–insoluble (junctional, top) and –soluble (nonjunctional, bottom), cell-surface, biotin-tagged Cx43 collected immediately after tagging (0 h) or following 2 h of treatment with Veh, αCT-1, or Rev posttagging. (B) The ratio of Triton X-100–insoluble to Triton X-100–soluble Cx43 is significantly increased by αCT-1 treatment. *$P = 0.002$ vs. 0 h; #$P = 0.011$ vs. Rev; N = 3 experiments, which represent densitometry from one blot per experiment. Error bars represent SEM.

effects on other junction types that might confound the results (Ryeom *et al.*, 2000). Similar to αCT-1–treated cells, when ZO-1 siRNA–transfected cells were subjected to gap-FRAP, fluorescence recovery occurred much faster than scrambled (Sc) siRNA–transfected controls (Figure 6D). Also as with αCT-1–treated cells, nonlinear regression indicated a modest elevation in F_∞ value compared with Sc siRNA control (Figure 6E). The rate of recovery (k) was also greater for ZO-1 siRNA–treated cells, and the increase was statistically significant (Figure 6F).

We conclude that reduction of ZO-1 levels increases GJIC in a manner that is not attributable to changes in Cx43 expression. The ZO-1 loss-of-function effects on GJIC were moreover consistent with those mediated by the PDZ2-binding peptide, indicating that increased GJ aggregation over the 2 h time course resulted in increased levels of cell-to-cell communication.

Connexon activity is reduced by inhibition of the Cx43/ZO-1 interaction

On the basis of our biotin-tagging experiment (Figure 3), an expected functional correlate of increased communication over the 2 h time course is a complementary decrease in connexon activity. Cell-surface connexon-mediated permeance was measured by ethidium bromide (EtdBr) uptake assay. In this assay, EtdBr in the media was taken up by cells, and EtdBr fluorescence was measured either during live imaging (Figure 7) or in cells fixed after a 15 min incubation (Figure 8).

The assay of single membrane connexon (hemichannel) activity was performed in both confluent monolayer cultures (Figure 7, A, B, and D) and low-density cultures, which allowed for the evaluation of
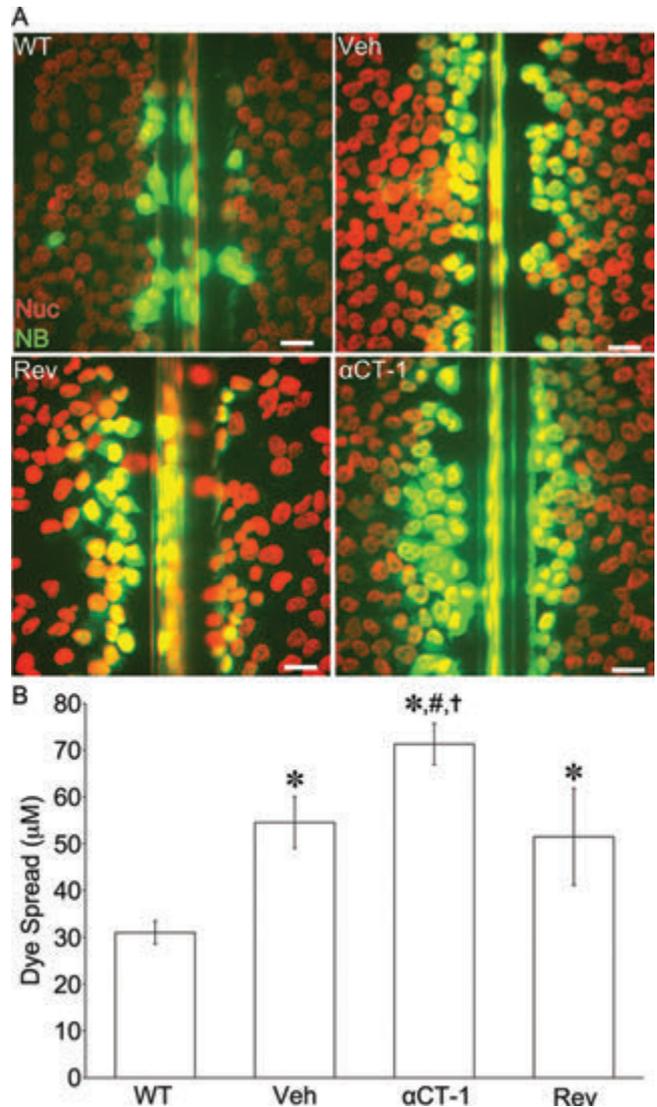

FIGURE 4: αCT-1 increases GJIC as assayed by scrape loading. (A) Representative images of neurobiotin (NB; green) in scrape-loaded wild-type HeLa cells (i.e., not expressing Cx43) and Veh-, αCT-1–, and Rev-treated Cx43-Hela cells (correspondingly labeled WT, Veh, αCT-1, and Rev in the images). The nuclear labeling has been changed to red for clarity; scale bars = 25 μm. (B) Cx43-HeLa cells from all treatment groups transfer dye further than WT HeLa cells: *$P < 0.03$. N = 8 for WT, Veh, and αCT-1; N = 3 for Rev. Additionally, αCT-1–treated cells display significantly greater communication than control Cx43-HeLa cells: #$P = 0.016$ vs. Veh; †$P = 0.032$ vs. Rev. N numbers indicate the number of experiments performed in which the distance of dye spread was calculated from measurements taken from two replicates per treatment. Four images were examined from each replicate, and two measurements were taken from each image (one from each side of the scratch). Error bars represent SEM.

isolated, noncontacting cells (Figure 7, A, C, and E). The rationale of the experiment was that while contacting Cx43-HeLa cells competently form GJs, isolated noncontacting cells are by definition unable to form cell–cell contacts. In noncontacting cells the total pool of membrane Cx43 should occur as undocked connexons that are unable to transition into GJs, and therefore their function should be unaffected by blocking the Cx43/ZO-1 interaction if ZO-1 inhibits connexon recruitment.
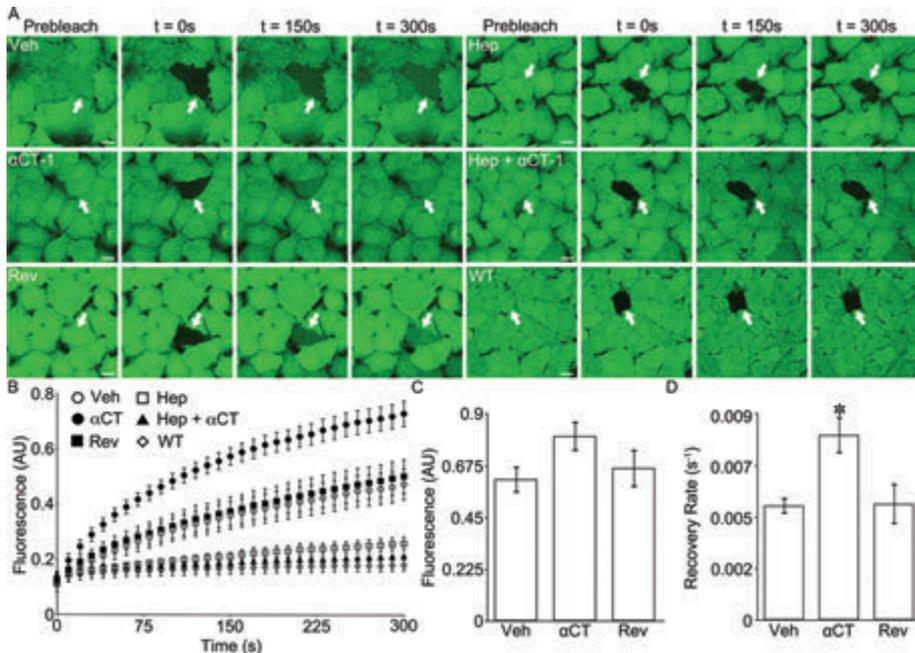
FIGURE 5: Inhibition of Cx43/ZO-1 increases the rate of recovery in a gap-FRAP model of GJIC. (A) Fluorescent images of calcein green fluorescence in wild-type (WT) and Cx43-HeLa cell monolayers before bleaching (Prebleach), just after bleaching (t = 0 s), and halfway through and at the end of the recovery period (t = 150 and 300 s, respectively). The Cx43-HeLa cells are treated with either vehicle (Veh), αCT-1, reverse control peptide (Rev), heptanol (Hep), or heptanol with αCT-1 (Hep + αCT). Arrows indicate the location of the bleached cell. Scale bar = 15 μm. (B) Gap-FRAP plot of bleached cell fluorescence during 300 s postbleaching. (C and D) Nonlinear regression of fluorescence data to an exponential decay function yielded values for (C) F_∞ (maximal predicted fluorescence recovery) and (D) k (rate of recovery). *P < 0.02 vs. all other groups; N = 4 experiments, which are determined from three bleach fields for each treatment in each experiment. Error bars represent SEM for all panels.

Confluent monolayers of vehicle and reverse control peptide–treated Cx43-HeLa cells took up EtdBr at a significantly greater rate than wild-type HeLa monolayers (Figure 7, B and D). However, αCT-1–treated Cx43-HeLa cell monolayers of contacting cells displayed a significantly lower rate of uptake compared with Cx43-expressing controls, and only slightly greater than wild-type HeLa cells (Figure 7, B and D). Importantly, noncontacting Cx43-HeLa cells did not display markedly different uptake from one another, although Cx43-HeLa cells took up EtdBr significantly faster than wild-type HeLa cells regardless of treatment (Figure 7, C and E). These results indicate that disruption of the Cx43/ZO-1 interaction reduces connexon activity in a manner that is dependent on the presence of GJs for connexons to transition into, or at least the ability to form GJs as would be present when cells are in close contact. Thus disruption of the Cx43/ZO-1 interaction in the absence of GJ formation had no effect on connexon function.

Based on the live-imaging data, the 15 min time point was studied for connexon activity in greater detail. Cx43-HeLa cell cultures treated with αCT-1 showed a significant drop in connexon activity compared with both vehicle and reverse controls (Figure 8A). To confirm that Cx43-HeLa cell EtdBr uptake beyond that displayed by wild-type HeLa cells is Cx43 connexon specific, Cx43-HeLa and wild-type HeLa cells were tested for response to EGTA, a connexon activator (Li et al., 1996; Saez et al., 2005); 18-β-glycyrrhetinic acid (BGA), a connexon blocker (Contreras et al., 2003); and mefloquine (MFQ), another connexon blocker as outlined by others in the Cx43 hemichannel literature (Tong et al., 2007).

BGA and MFQ reduced Cx43-HeLa cell connexon activity, while wild-type HeLa cell EtdBr uptake was unaffected by either inhibitory MFQ or BGA treatments (Figure 8B). Conversely, EGTA significantly increased cell-surface connexon function in Cx43-HeLa cells but not wild-type HeLa cells (Figure 8C). Furthermore, wild-type HeLa cells treated with vehicle, αCT-1, and reverse control peptide did not show significant differences in uptake, indicating that the effects of αCT-1 were dependant on expression of Cx43 (Figure 8A). These results corroborate the live-imaging assay of connexon activity, and we conclude that EtdBr uptake by Cx43-HeLa cells was 1) Cx43 dependent and 2) connexon mediated and 3) that the effects of αCT-1 were Cx43 connexon specific. Most importantly, as predicted from Figure 3, αCT-1 treatment reduced membrane permeance consistent with a reduction in the surface density of connexons.

EtdBr uptake was also measured in the context of ZO-1 knockdown by siRNA as an alternative means of reducing Cx43/ZO-1 interaction. Uptake assays were performed in parallel with gap-FRAP experiments described previously. Consequently, the Western blot analysis of Cx43 and ZO-1 levels shown in Figure 6 applies to this part of the study. Similar to disruption of the Cx43/ZO-1 interaction by αCT-1, ZO-1 siRNA treatment significantly decreased EtdBr uptake compared with Sc siRNA control (Figure 8D). These results support the αCT-1 data and show that ZO-1 expression has a direct effect on the level of hemichannel activity mediated by undocked connexons in the plasma membrane.

DISCUSSION

A physiological role for ZO-1 interaction with Cx43 is resolved in regulating the transition of undocked connexons into GJ aggregates of intercellular channels. This finding extends our previous work in which we concluded that ZO-1 governed trafficking between nonjunctional and junctional pools of Cx43 (Hunter et al., 2003, 2005). What is new here is that we 1) identify a previously unknown region around GJ plaques where Cx43/ZO-1 interaction concentrates—the perinexus; 2) show that the changes in the nonjunctional fraction of Cx43 induced by disruption of the Cx43/ZO-1 interaction correspond to shifts in cell-surface connexons and not cytoplasmic pools of nonjunctional Cx43; and 3) determine that ZO-1 regulation of the connexon to GJ transition occurs at a rate comparable to that at which connexons are incorporated in and removed from the plasma membrane, as deduced from Cx43 half-life (Laird et al., 1991; Laird, 1996; Darrow et al., 1995; Saffitz et al., 2000; Hunter et al., 2005).

These findings provide a framework for understanding how Cx43 may switch, in a dynamically regulated manner, between distinct roles in the plasma membrane. Our results suggest that Cx43/ZO-1 interaction proximal to the GJ governs partitioning of the connexon function between hemichannels within the perinexus and intercellular channels mediating GJIC. Figure 9 provides a model of how
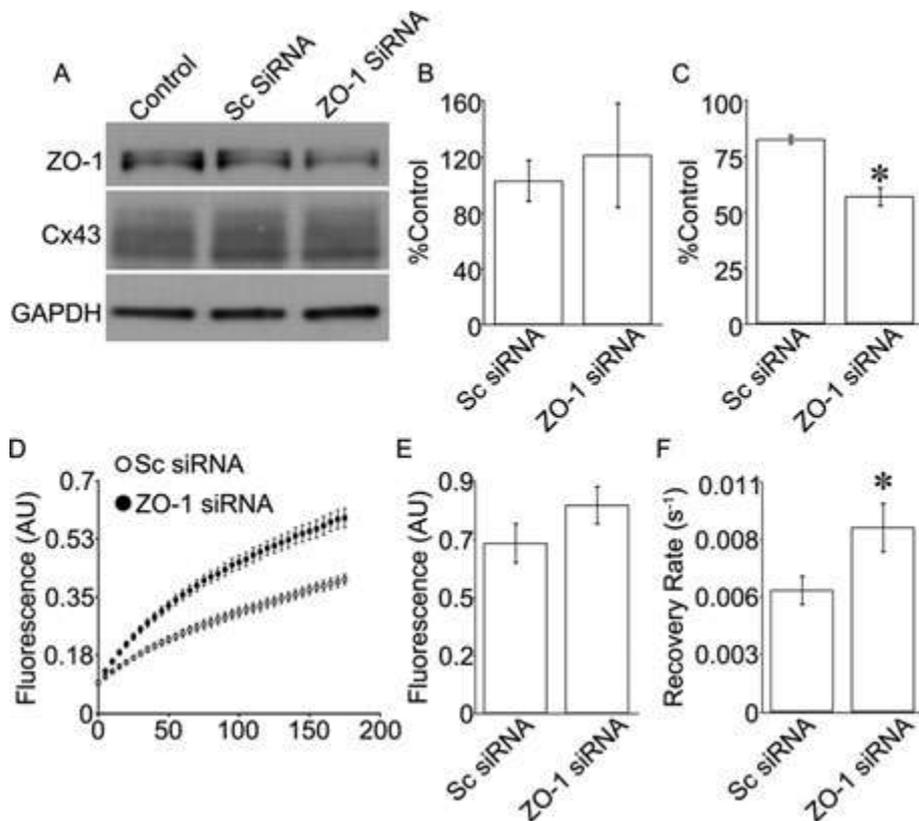
FIGURE 6: ZO-1 siRNA knockdown mimics the effects of αCT-1. (A) Representative blots of ZO-1, Cx43, and glyceraldehyde-3-phosphate dehydrogenase from Cx43-HeLa cells under control conditions or transfected with either Sc siRNA or ZO-1 siRNA. (B and C) Densitometric analysis of (B) Cx43 protein levels shows no statistical difference between Sc and ZO-1 siRNA–transfected cells, whereas (C) ZO-1 levels are significantly reduced by ZO-1 siRNA, *P = 0.002; N = 4 separate cultures transfected with ZO-1 siRNA. (D) Gap-FRAP plot of bleached cell fluorescence during 175 s postbleaching from Sc siRNA– or ZO-1 siRNA–transfected Cx43-HeLa monolayers. (E and F) Nonlinear regression to fluorescence data yielded values for (E) maximal predicted recovery, F_∞, and (F) the rate constant, k. *P = 0.05; N = 3 experiments performed on three cultures transfected in parallel with those analyzed in A–C. Measurements were determined from three separate bleach fields in each experiment from each treatment condition. Error bars represent SEM for all panels.

ZO-1 may act to variably inhibit connexon recruitment via its interaction with the Cx43 CT.

Previous work from our laboratory demonstrated that disruption of the Cx43/ZO-1 interaction increases GJ size (Hunter et al., 2003, 2005). One approach used in these earlier studies involved expression of a Cx43–green fluorescent protein (GFP) fusion protein incompetent to interact with ZO-1. While providing useful insight, constitutive expression of Cx43-GFP precluded temporal resolution of the effect of the interaction on GJ biogenesis (Hunter et al., 2003). Similarly, a second approach involved a prolonged inhibition of the Cx43/ZO-1 interaction by exposure of Cx43-expressing HeLa cells or cardiomyocytes to the PDZ2-binding peptide αCT-1 over a 48 h period (Hunter et al., 2005).

Given the rapid turnover rate of Cx43, it was reasoned that if the canonical pathway of GJ accretion from hemichannels diffusing laterally in the membrane is correct (Martin and Evans, 2004; Thomas et al., 2005; Laird, 2006), then ZO-1 regulation of GJ size likely operates over periods of <48 h. This premise was tested by examining the effect of disrupting Cx43/ZO-1 binding over 2 h—an interval on the same order as the Cx43 half-life (Laird et al., 1991; Laird, 1996; Darrow et al., 1995; Saffitz et al., 2000; Hunter et al., 2005). It was found that GJ aggregate size indeed increased over 2 h in response

to αCT-1. In concert with GJs becoming larger over 2 h, the ratio of biotin-tagged Cx43 in GJs to nonjunctional cell-surface Cx43 increased. The confocal and biochemical data strongly supported the concept that binding of the Cx43 CT to ZO-1 limits the rate at which undocked connexons in the plasma membrane incorporate into GJ plaques. Moreover, these results place ZO-1 at the GJ periphery as part of a dynamic mechanism for apportioning connexons between hemichannel and intercellular channel functions.

Studies undertaken in transgenic mice (Maass et al., 2007) and with tissues from human patients with heart disease (Bruce et al., 2008) have provided further evidence that ZO-1 has a role in regulating the extent of GJ aggregates in vivo. Maass, Delmar, and coworkers demonstrated that mice expressing a CT-truncated Cx43, incompetent to interact with ZO-1, formed GJs at cardiac IDs that were larger than those observed in wild-type litter mates (Maass et al., 2007). Bruce et al. (2008) reported that ZO-1 levels were significantly increased at ventricular IDs in heart failure patients. As would be anticipated from the effects of loss of the Cx43/ZO-1 interaction in the current study, these workers found that a gain in Cx43/ZO-1 association in congestive heart failure patients was correlated with increased remodeling and decreased size of Cx43 GJs. The results of Bruce et al. are also in line with our demonstration that ZO-1 overexpression and increased Cx43/ZO-1 interaction result in decreased Cx43 GJ size—a remodeling event associated with generation of an arrhythmic substrate in patients with heart failure (Severs et al., 2008).

The immunoprecipitation and Duolink assay data provide further new insight into the mechanistic function of the Cx43/ZO-1 interaction. The results suggest that ZO-1 interacts with both connexons and GJ-associated intercellular channels but that only junctional Cx43 interacts with cytoskeletal actin (Fox et al., 1993). The Cx43/ZO-1 interaction within the perinexus, as visualized by Duolink, did not coincide with actin or Cx43 immunofluorescence. Therefore we infer that Cx43 molecules within this region are in the form of connexons. Furthermore, αCT-1 treatment of cultures extensively reduced GJ-associated Cx43/ZO-1 interaction and decreased the relative proportion of plasma membrane connexons, indicating that ZO-1 binding of Cx43 in the perinexus acts as a barrier (albeit porous) to connexon incorporation into GJs at the plaque edge.

The edge of the GJ has come into focus in recent years as a site for interactions between connexins and their partnering proteins (Hunter et al., 2005; Hunter and Gourdie, 2008; Zhu et al., 2005; Akoyev and Takemoto, 2007; Baker et al., 2008; Gilleron et al., 2008; Kieken et al., 2009). In this article we provide evidence that Cx43, ZO-1, and actin interact within the GJ multiprotein complex. It is also shown that a domain of the Cx43/ZO-1 interaction—not including bound actin—extends from the GJ into the connexon-containing perinexal region. The perinexus represents a previously
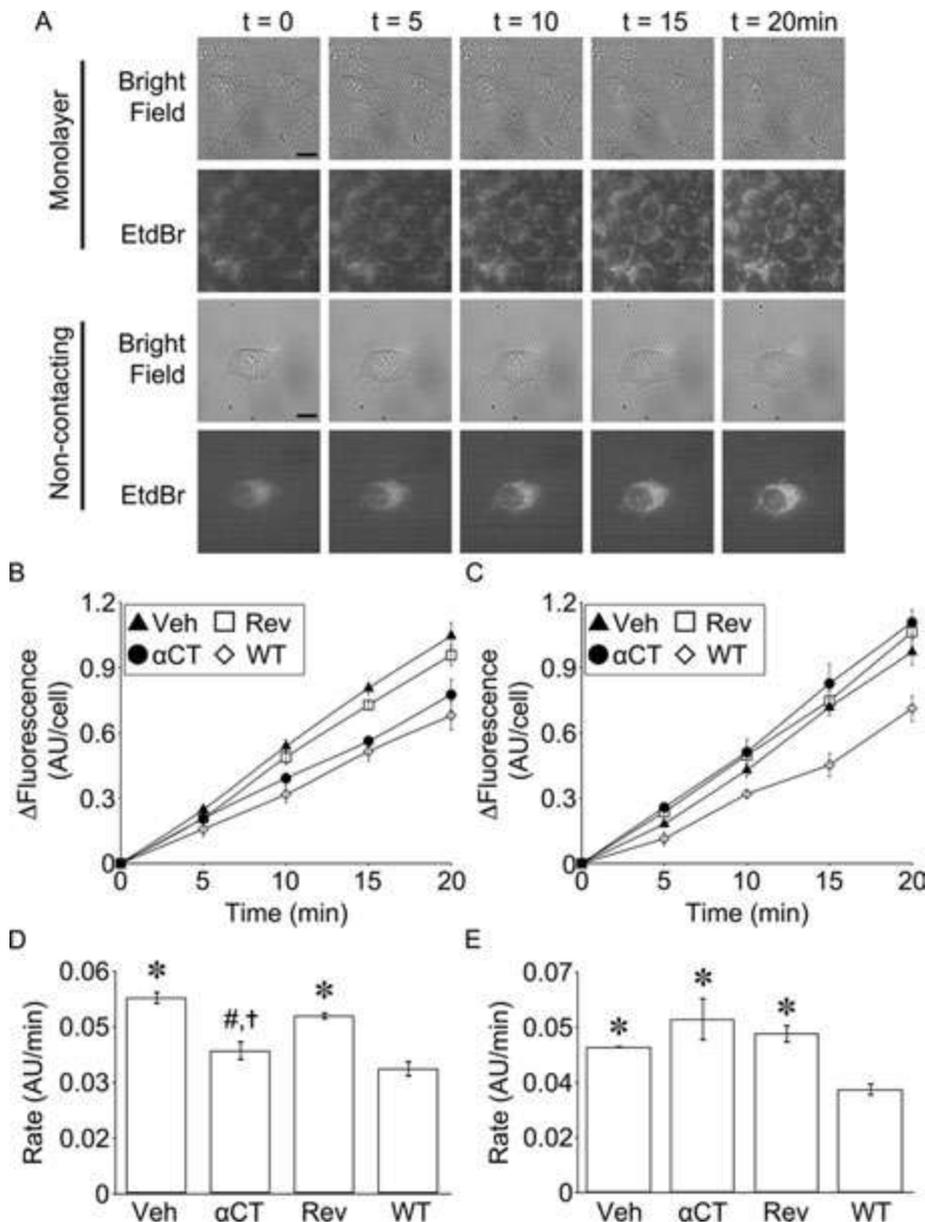
FIGURE 7: Disruption of the Cx43/ZO-1 interaction reduces the rate of EtdBr uptake in Cx43-HeLa cell monolayers but not individual, noncontacting cells. (A) Representative images from a live-cell EtdBr uptake experiment performed on vehicle (Veh)–treated Cx43-HeLa cell monolayers or single cells during 20 min. Scale bar = 15 μm. (B and C) Plots of measured EtdBr fluorescence change over a 20 min period from (B) monolayers or (C) individual wild-type HeLa (WT) cells and Cx43-HeLa cells treated with Veh, αCT-1, or reverse control peptide (Rev). (D and E) Statistical analysis of rate data from B and C, respectively. (D) *P < 0.002 vs. WT; #P = 0.001 vs. Veh; †P = 0.009 vs. Rev; N = 3. (E) *P < 0.02 vs. WT; N = 3. Error bars represent SEM for all panels. N numbers for both monolayer and noncontacting cultures indicate the number of separate experiments performed in which six different fields were monitored and EtdBr uptake was quantified.

The model described in Figure 9 appears to contrast to that provided in the elegant report of Shaw, Jan, and coworkers (Shaw et al., 2007). They proposed a cytoplasmic mechanism for direct delivery of connexons to GJs. In this model, microtubules trafficking connexons are linked by plus ends to N-cadherin at GJs. Supporting this, the group demonstrated that fluorescence recovery of Cx43-YFP–tagged GJs following photobleaching (i.e., FRAP of yellow fluorescent protein) in HeLa cells recovered uniformly across GJs and not preferentially at plaque edges. This suggested that Cx43 was targeting directly into GJs, rather than being recruited from the surrounding membrane to the GJ edge by lateral diffusion of connexons. The FRAP results also indicated that approximately one-third of the plaque recovered in <5 min.

It is notable that other workers utilizing FRAP of Cx43 GJs or successive labeling of tetracysteine-tagged Cx43 have not reported rapid kinetics for accretion of connexons similar to those reported originally by the Jan group (Gaietta et al., 2002; Lauf et al., 2002). Rather, the rates of FRAP and/or Cx43 recruitment found in these studies appear to be consistent with what might be anticipated from the 1–3 h half-life of Cx43 and the new data that we provide here. These studies also place the location of Cx43 recruitment at the plaque periphery (Gaietta et al., 2002; Lauf et al., 2002; Thomas et al., 2005; Laird, 2006). Importantly, this is also where we and others have identified the primary site of ZO-1 localization at GJs (Hunter et al., 2005; Zhu et al., 2005; Akoyev and Takemoto, 2007; Baker et al., 2008; Gilleron et al., 2008; Kieken et al., 2009).

There is evidence that rapid assembly of connexons into GJs occurs under certain circumstances (Hendrix et al., 1992; Paulson et al., 2000; Martin and Evans, 2004). It is also noteworthy that similar to Cx43-GFP, the Cx43-YFP fusion protein used by Shaw and colleagues would be expected to be incompetent to bind ZO-1 (Hunter et al., 2003). It follows from this that a trafficking pathway dependent on the Cx43/ZO-1 interaction would have not been resolved.

It may also be pertinent that ZO-1 localizes at both N-cadherin–containing adherens junctions and Cx43 GJs (Gonzalez-Mariscal et al., 2000). This raises the prospect of a role for ZO-1 as an intermediary colocalizing the two junction types. Thus, while our results are difficult to reconcile with rapid, uniform targeting of Cx43 across the GJ, the data may be consistent with a variant of the Shaw model embodied in the mechanism outlined in Figure 9. In this model, it could be envisaged that adherens junctions nearby to GJs act as sites of preferential delivery of connexons to nonjunctional plasma membrane proximal to GJs (i.e., the

unrecognized nidus proximal to GJs for functionally significant interactions between membrane, junctional, and signal transduction molecules. For example, the GJ represents one of the closest approximations between the plasma membranes of two cells. Anchorage of hemichannels in the perinexus may thus provide a novel, ephapse-like locus for cell-to-cell signaling. New avenues for future work on cellular regulation and signaling may be opened up by the identification of this novel feature of membrane ultrastructure.
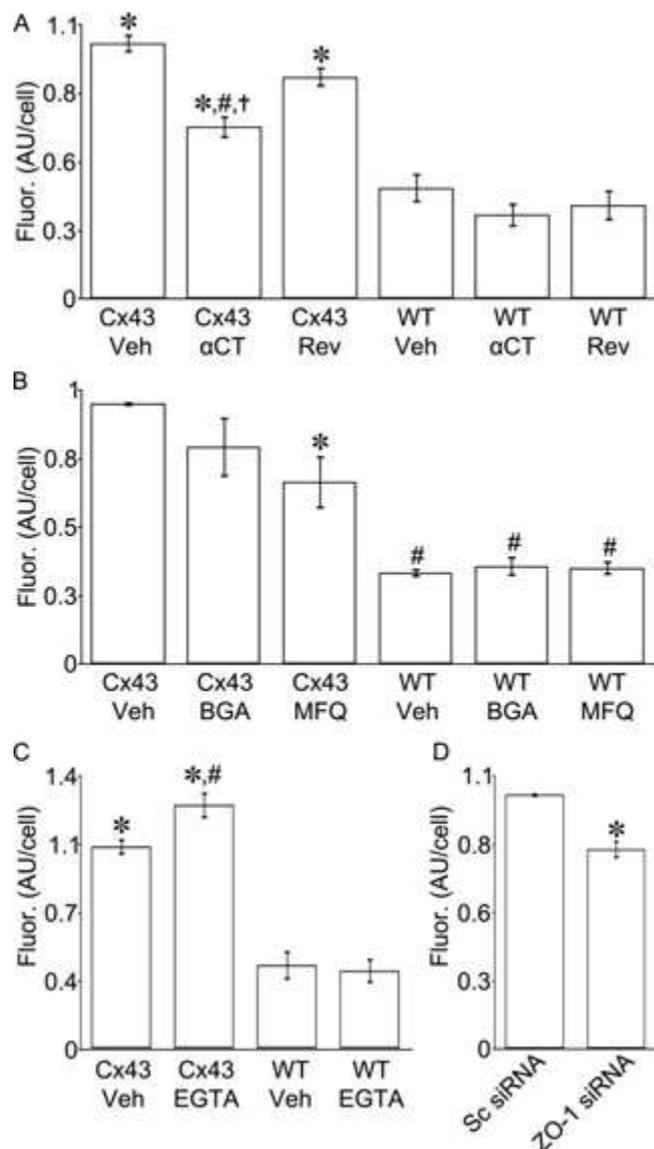
FIGURE 8: ZO-1 knockdown and αCT-1 both inhibit EtdBr uptake in a hemichannel-specific manner. (A) EtdBr taken up after 15 min in monolayers of Cx43- and wild-type HeLa (WT) cells treated with vehicle (Veh), αCT-1, or reverse control peptide (Rev). *P < 0.004 vs. any treatment of WT HeLa cells; #P = 0.0002 vs. Veh; †P = 0.011 vs. Rev; N = 4. (B) EtdBr taken up after 15 min in monolayers of Cx43- and WT HeLa cells treated with Veh, BGA, or MFQ. *P = 0.037 vs. Veh; #P < 0.0004 vs. Veh; N = 3. (C) EtdBr taken up after 15 min in monolayers of Cx43- and WT HeLa cells treated with Veh or EGTA. *P < 0.0001 vs. any treatment of WT HeLa cells; #P = 0.02 vs. Veh; N = 15, 11, and 4 for Cx43-HeLa Veh, Cx43-HeLa EGTA, and both WT HeLa treatments, respectively. (D) EtdBr taken up after 15 min in monolayers of Cx43-HeLa cells treated with either Sc siRNA or ZO-1 siRNA. *P = 0.02; N = 3. N numbers indicate the number of experiments performed in which measurements were taken on five images per experiment for each treatment type. Error bars represent SEM for all panels.

perinexus). Undocked connexons reaching the plasma membrane via microtubule/N-cadherin complexes would then accrete to GJs subject to the frequency with which Cx43 CTs encountered ZO-1 near the GJ edge. A notable unknown in this model would be when and how the actin cytoskeleton engaged connexons linked to ZO-1 during their transition into GJs.

Our data indicate that levels of GJIC and hemichannel permeability vary in inverse and direct proportion to levels of ZO-1/Cx43 interaction, respectively. Loss of the Cx43/ZO-1 interaction via αCT-1 or ZO-1 antisense resulted in decreased membrane permeability by hemichannels and increased GJIC. An important observation is that αCT-1 did not alter EtdBr uptake in noncontacting cells unable to form GJs. This experiment indicates that affects on hemichannel function by the PDZ2-binding peptide were likely not due to changes in channel gating. This is because plasma membrane connexon density and hemichannel permeance remained unchanged in the absence of the opportunity for connexons to aggregate into GJs. Preliminary electrophysiological studies also support the concept that αCT-1 is not likely to have direct effects on hemichannel gating (Rhett, Gourdie, and Morad, unpublished data). Further support of this is evidenced in our finding that αCT-1 did not affect phosphorylation of Cx43 on Ser-368 (Supplemental Figure 3), a known modulator of channel gating (Ek-Vitorin et al., 2006). A novel inference from our work is that the connexon-containing perinexus is a membrane domain, specialized for hemichannel function. Future high-resolution studies of channel function will be needed to confirm this hypothesis.

Overall, the findings provided herein on Cx43 hemichannel function compare well with the studies of Saez, Bennet, and colleagues (Contreras et al., 2003; Retamal et al., 2007). Similar to what we report here, these workers have shown that the rate of hemichannel-mediated EtdBr uptake is linearly related to the level of Cx43 expression. Our data also confirm their finding that blockers of GJIC inhibit connexon activity and that low Ca^{2+} increases hemichannel function.

The changes in membrane permeability brought about by modulation of the Cx43/ZO-1 interaction may have important physiological consequences. As discussed by Bukauskas and coworkers (Kreuzberg et al., 2006), hemichannels may serve to depolarize the excitable membranes of myocytes by reducing the space constant. In addition to reduction in the space constant, increases in hemichannel density may alter membrane voltage potential and promote cell death and ATP release, all of which are arrhythmogenic (Kreuzberg et al., 2006; Shintani-Ishida et al., 2007; Clarke et al., 2009). Therefore, in addition to providing mechanistic insight into the contribution of hemichannel dysfunction to injury and disease, the data presented herein supply a basis for the creation of new molecular medicines. Indeed, work by O'Quinn et al. (2011) from our laboratory has shown that application of αCT-1 to infarcted myocardium results in a reduction in the severity of arrhythmias induced by ex vivo–stimulated pacing protocols. Further work is required to determine whether this decreased propensity for induced arrhythmia is associated with reductions in hemichannel activity similar to those that we describe here in vitro in response to the Cx43 PDZ2-binding domain.

In conclusion, it was found that ZO-1 interaction with the Cx43 CT dynamically governs the rate of GJ accretion from connexons in the perinexus, with attendant affects on hemichannel function. Our work suggests a novel cellular mechanism by which membrane permeability and intercellular communication are coordinately regulated—a mechanism that may become dysregulated in cardiac disease, with potential implications for the genesis of electrical conduction disturbance (Bruce et al., 2008; Severs et al., 2008). Interestingly, other PDZ proteins function in dynamically regulating channel transitions between disaggregated and aggregated assemblies, for example, PSD95 and AMPA receptors at synapses (Bats et al., 2007). Of further note is that connexins have been shown to have roles in intercellular adhesion (Lin et al., 2002; Elias et al., 2007; Cotrina et al., 2008). In ongoing studies it will therefore be of
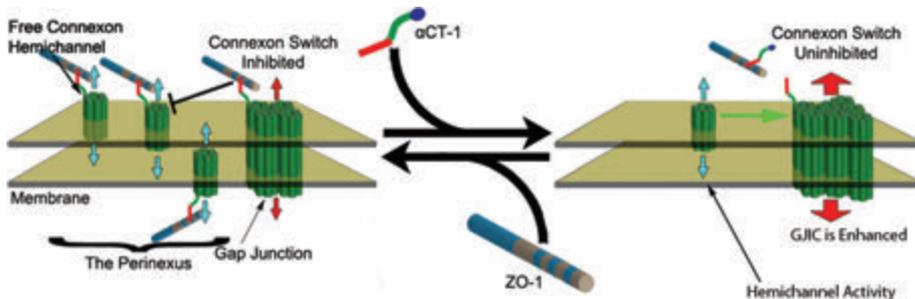
FIGURE 9: The connexon switch. When ZO-1 is bound to Cx43 at the periphery of GJ plaques and hemichannels in the perinexus—"connexon switch inhibited"—hemichannel addition to the plaque perimeter is restricted. When Cx43/ZO-1 interaction is inhibited (as with αCT-1)—"connexon switch uninhibited"—GJ accretion from hemichannels is unchecked, resulting in larger GJs and fewer hemichannels. The predicted functional consequences of disengaging Cx43 and ZO-1 are greater GJIC (red arrows) and reduced hemichannel activity (blue arrows).

interest to determine whether ZO-1 modulation of the transition of undocked connexons into GJs provides a means for dynamically regulating levels of both coupling and adhesion between cells.

MATERIALS AND METHODS

Antennapedia peptides and cell culture

Peptides were generated as previously described (Hunter *et al.*, 2005): αCT-1 and a reverse sequence control peptide (Rev). Both contain an N-terminal biotin tag followed by the 16–amino acid antennapedia internalization vector (RQPKIWFPNRRKPWKK). Linked to the CT lysine of the antennapedia sequence is either the CT 9 amino acids of Cx43 (RPRPDDLEI; αCT-1) or the Cx43 CT 9 amino acids in reverse (IELDDPRPR; Rev). Peptides were used at a concentration of 180 μM. Parental wild-type HeLa cells (ATCC, Manassas, VA), HeLa cells stably expressing Cx43 (Cx43-HeLa; a generous gift from Klaus Willecke), and HeLa cells stably expressing Cx43–enhanced green fluorescent protein (EGFP) (Cx43-EGFP-HeLa; Jordan *et al.*, 1999) were cultured as previously described (Hunter *et al.*, 2005). RECs were kindly provided by Hoda Eid and induced to stably express Cx43-EGFP by electroporation with a Cx43-EGFP expression vector (Jordan *et al.*, 1999), followed by selection with G418.

Transient transfection

For ZO-1 overexpression, cells were transfected with a DsRedC1–huZO-1 (human ZO-1 N-terminally tagged with DsRed) construct using Lipofectamine Plus (Invitrogen, Carlsbad, CA; Cat. no. 15338100) according to the manufacturer's instructions. For ZO-1 knockdown, cells were transfected with either control Sc siRNA or ZO-1 siRNA (a mixture of three different oligonucleotides targeting ZO-1 mRNA) according to the manufacturer's instructions (Santa Cruz Biotechnology, Santa Cruz, CA; Cat. no. sc-29829).

Immunocytochemistry, image acquisition, and analysis

Cx43 was stained using an anti-Cx43 antibody (Santa Cruz Biotechnology, Cat no. SC-6560). Actin was labeled by Alexa Fluor 647 phalloidin (Invitrogen; Cat. no. A22287). The Cx43/ZO-1 interaction was detected in situ using the Duolink II secondary antibodies and detection kit (Olink Bioscience, Uppsala, Sweden; Cat. nos. 92001, 92005, and 92007) according to manufacturer instructions. Briefly, primary antibodies against Cx43 (Millipore, Danvers, MA; Cat no. MAB3067) and ZO-1 (Invitrogen; Cat. no. 617-300) were applied under standard conditions. Duolink secondary antibodies against the primary antibodies were then added. These secondary antibodies were provided as conjugates to oligonucleotides that were li-

gated together in a closed circle by Duolink Ligation Solution, if the antibodies were in close proximity (<40 nm; Gullberg, 2010). Finally, polymerase was added, which amplified any existing closed circles, and detection was achieved with complementary, fluorescently labeled oligonucleotides. The specificity of this assay was assessed by staining of Cx43-EGFP-HeLa cells (i.e., these cells express only Cx43 incapable of interacting with ZO-1 [Hunter *et al.*, 2003]; Supplemental Figure 1). Confocal images were acquired on a TCS SP5 laser scanning confocal microscope (LSCM) equipped with a 63×/1.4 numerical aperture (NA) oil objective (Leica, Buffalo Grove, IL). GJ size was analyzed, as previously described (Hunter *et al.*, 2005), by creating a mask of cell borders based on actin (αCT-1 experiments) or ZO-1 (ZO-1 overexpression experiments) staining followed by measurement of Cx43 staining within the mask using ImageJ software (version 1.42q; National Institutes of Health [NIH], Bethesda, MD). The mask was generated using the pencil tool with 20 pixel line width by tracing over cell borders highlighted by cortical actin staining. Positive Cx43 staining was defined as pixels with 128–255 gray value, and positive Duolink stain was defined as pixels with 137–255 gray value (8-bit images). Duolink stain was also measured by counting the total number of positive pixels and the number of positive pixels under the membrane mask. Colocalization analysis was performed using the Colocalization Analysis plug-in in the McMaster Biophotonics Facility version of NIH ImageJ found at www.macbiophotonics.ca/downloads.htm. Colocalization was calculated as the percentage of total Cx43 pixels that were colocalized with ZO-1.

Immunoprecipitation

Cx43-HeLa cell lysates were separated into junctional and nonjunctional Cx43 fractions based on detergent solubility per the method of Musil and Goodenough (1991). Cells were lysed in the presence of 1% Triton X-100 (Fisher Scientific, Pittsburgh, PA; Cat. no. BP151) and clarified by centrifugation at 100,000 × *g* for 50 min at 4°C. Immunoprecipitation was then performed on the two fractions using ZO-1 antibody (Santa Cruz Biotechnology; Cat. no. SC-10804) or control rabbit immunoglobulin (Ig) G (Jackson ImmunoResearch Laboratories, West Grove, PA; Cat. no. 011-000-003) coupled to nProtein A Sepharose Fast Flow beads (Amersham, Uppsala, Sweden; Cat. no. 17-5280-01). Proteins from whole lysates, fractions, and immunoprecipitation reactions were resolved by 10% SDS–PAGE (Bio-Rad, Hercules, CA; Cat. no. 345-0111) followed by immunoblotting with Cx43 antibody (Sigma, St. Louis, MO; Cat. no. C-6219). Immunoblotted proteins were detected using a horseradish peroxidase–conjugated secondary antibody against rabbit IgG light chain (Jackson ImmunoResearch; Cat. no. 211-052-171) to minimize detection of the antibody used for immunoprecipitation. Signal was detected by bioluminescence as previously described (Hunter *et al.*, 2005). These blots were then stripped with β-mercaptoethanol and reprobed using an actin antibody (Millipore; Cat. no. MAB1501) or ZO-1 antibody (Invitrogen; Cat. no. 617300).

Cell-surface biotin tagging, pull-down, Triton X-100 fractionation, and Western blotting

Cell-surface proteins were tagged with biotin using the general methodologies described by Musil and Goodenough (1991) and VanSlyke

and Musil (2005): Confluent Cx43-HeLa cells were incubated with 0.5 mg/ml sulfo-NHS-LG-biotin (Thermo Scientific, Rockford, IL; Cat. no. 21338) in Dulbecco's phosphate-buffered saline (DPBS; Invitrogen; Cat. no. 14080-055), pH 8.0, for 15 min at 4°C, rotating slowly. Unreacted biotin was quenched with 15 mM glycine (Fisher Scientific; Cat. no. BP381-1) in DPBS, pH 8.0. Cells were either lysed immediately or treated with vehicle (Veh; Opti-MEM; Invitrogen; Cat. no. 11058-021), αCT-1, or reverse control peptide and returned to incubation for 2 h followed by lysis. Junctional and nonjunctional Cx43 were separated as described above. Fractions were then run on 10-kDa molecular weight cutoff columns (Millipore; Cat. no. UFC801024) followed by purification of biotin-tagged protein on NeutrAvidin beads (Fisher Scientific; Cat. no. PI29201). Biotin-tagged protein was eluted with 8 M guanidine (Sigma; Cat. no. G4505), and guanidine was removed by centrifugation on Zeba Desalt columns (Thermo Scientific; Cat. no. 89894). Proteins were resolved by 10% SDS–PAGE (Bio-Rad; Cat. no. 345-0111) followed by immunoblotting with Cx43 antibody (Sigma; Cat. no. C-6219). For ZO-1 knockdown experiments, cells were lysed and proteins from lysates were resolved by either 10% SDS–PAGE (Bio-Rad; Cat. no. 345-0111; Cx43 and pS368) or 7% SDS–PAGE (Bio-Rad; Cat. no. 345-0135; ZO-1) followed by immunoblotting with Cx43 antibody (Sigma; Cat. no. C-6219), phospho-Cx43-S368 antibody (Cell Signaling, Danvers, MA; Cat. no. 3511s), or ZO-1 antibody (Invitrogen; Cat. no. 617300). Immunoblotted proteins were detected using a horseradish peroxidase–conjugated secondary antibody as previously described (Hunter et al., 2005).

Assays of GJIC

For scrape-loading GJIC, the method used was based on that of Yum et al. (2007): Confluent wild-type and Cx43-HeLa cells were exposed to either vehicle (Veh; Opti-MEM), αCT-1, or reverse control peptide for 2 h in culture conditions. Cells were then washed with Hank's balanced salt solution without Ca^{2+} or Mg^{2+} (HBSS$^-$; Invitrogen; Cat. no. 14175-095), and then 2% neurobiotin (Vector Laboratories, Burlingame, CA; Cat. no. SP-1120) in HBSS$^-$ was added to the cells. Each well was scraped twice with a no. 11 scalpel, and cells were incubated for 5 min at 37°C, 5% CO_2. Cells were washed with HBSS$^-$, fixed for 10 min in 2% paraformaldehyde (Fisher Scientific; Cat. no. 04042-500) at room temperature, and blocked with 1% bovine serum albumin (EMD Chemicals, Gibbstown, NJ; Cat. no. 2930) and 0.1% Triton X-100 (Fisher Scientific; Cat. no. BP151) in PBS (Sigma; Cat. no. P4417). Cells were stained with streptavidin Alex Fluor 488 conjugate (Invitrogen; Cat. no. S32354; neurobiotin labeling) and Hoechst 33258 (Sigma; Cat. no. B2883; nuclear labeling). Cells were imaged on a Leica DM LB fluorescence microscope equipped with a 20×/0.50 NA water immersion objective. The distance of neurobiotin spread was determined using ImageJ by measuring the distance from the scrape edge to the point at which fluorescence intensity, averaged along a line parallel to the scrape edge, dropped below 150% that of the background.

The second assay of GJIC utilized, gap-FRAP, was based on that of Yum et al. (2007), with modification as follows: Confluent wild-type and Cx43-HeLa cells were incubated in Opti-MEM alone (wild-type and vehicle) or Opti-MEM plus αCT-1 or reverse control peptide for 2 h at 37°C, ambient CO_2. Cells were then loaded with 1 μM calcein green, AM (Invitrogen; Cat. no. C34852), by addition to the media for the final 30 min of the 2 h incubation. Cells were washed with PBS (Sigma; Cat. no. P4417), and Opti-MEM was added back to the cells, including 60 μM αCT-1 or reverse control peptide for appropriate cultures, and 3 mM heptanol (Alfa Aesar, Ward Hill, MA; Cat. no. A12973) for a subset of vehicle and αCT-1 treatments. Cultures were imaged on a TCS SP5 LSCM equipped with a 40×/0.80

NA water immersion objective using the Leica FRAP LAS-AF application wizard (Leica). Images were acquired once every 10 s for 5 min postbleaching (αCT-1 experiments) or once every 5 s for 3 min postbleaching (ZO-1 siRNA experiments). Fluorescence recovery of the bleached cell was measured using NIH ImageJ. The maximal recovery (F_∞) and rate constant (k) were determined using nonlinear regression performed on PASW Statistics, version 17.0.2 (IBM, Armonk, NY), using the following equation:

$$F(t) = F_0 + (F_\infty - F_0)(1 - e^{-t \cdot k}),$$

where t is the time after photobleaching, F(t) is the normalized fluorescence intensity, F_0 is the theoretical fluorescence intensity immediately after bleaching (estimated from the first postbleach image), F_∞ is the asymptotic theoretical maximal recovery value to which postbleach fluorescence intensity tends, and k is the rate constant. This exponential decay function is a commonly used model of GJ-mediated fluorescence recovery (Salmon et al., 1984; Abbaci et al., 2007, 2008).

Connexon function

Continuous live-cell imaging of EtdBr uptake. The procedure used to assay single membrane connexon-mediated permeance was based on the methods of Retamal et al. (2007). Confluent wild-type and Cx43-HeLa cells were incubated in Opti-MEM alone (wild-type and vehicle) or Opti-MEM plus αCT-1 or reverse control peptide for 2 h at 37°C, ambient CO_2. Immediately before imaging, 50 nM EtdBr (Sigma; Cat. no. E8751) was added to cultures. Cells were imaged on an Axiovert 200M microscope equipped with a 63×/1.4 NA oil objective (Carl Zeiss Microimaging, Thornwood, NY). Digital images of EtdBr fluorescence and bright field were captured of monolayers and isolated cells every 5 min over a 20 min period by an Orca ER CCD camera (Hamamatsu, Bridgewater, NJ) using Openlab 5.0.1 software (PerkinElmer, Waltham, MA). Images were analyzed by measuring the mean gray values of fluorescent images (entire field for monolayers and a region of interest of cell outline traced from bright-field images for noncontacting cells) using NIH ImageJ and normalizing to the number of cells in the field for monolayers.

Fixed time point assay of EtdBr uptake. The method of Shintani-Ishida et al. (2007) was adapted for this assay with modifications as described: Wild-type and Cx43-HeLa cell monolayers were scrutinized at a single 15 min time point by incubating as described previously for 2 h with either vehicle, αCT-1, or reverse control, then incubating with 500 nM EtdBr for 15 min, followed by fixation. For transfected cells, only the vehicle incubation was used. Controls included 4 mM EGTA (Sigma; Cat. no. E4378), 25 μM BGA (Sigma; Cat. no. G10105), and 25 μM MFQ (Sigma; Cat. no. M2319) in the solutions during the 15 min EtdBr incubation. Cells were fixed by washing with PBS with Ca^{2+} and Mg^{2+} (to ensure hemichannel closure) followed by a 10 min incubation with 2% paraformaldehyde (Fisher Scientific; Cat. no. 04042-500) at room temperature. Fixed monolayers were nuclear labeled with Hoechst 33258 (Sigma; Cat. no. B2883), mounted, and imaged within 24 h on a TCS SP5 LSCM equipped with a 63×/1.4 NA oil objective. EtdBr uptake was determined in these images by measuring the mean gray values of fluorescent images using NIH ImageJ and normalizing to the number of cells in the field.

Statistics

For GJ size analysis with αCT-1 treatment, measurements were taken from five images for each experiment. Three separate experiments were performed for αCT-1 GJ size/Duolink analysis and cell-surface

biotinylation assay. For the scrape-loading assay, each experiment was performed in duplicate, and four images each were taken along the scratch and outside the scratch in each replicate. Replicated scrape-loading experiments were performed a minimum of three times for each treatment group. Gap-FRAP statistics represent an average of three experiments. In each experiment, three separate fields were subjected to gap-FRAP over an ~20-min period. For the live-imaging assay, averages were determined from three experiments for each treatment group. Each experiment, in turn, was averaged from measurements of six distinct fields for each treatment group. Averages from the fixed-cell assay represent an average of at least three experiments. In each experiment, five separate fields were imaged. For multiple comparisons analysis of variance with post hoc analysis was performed. All statistics were prepared in PASW Statistics, version 17.0.2. N numbers are reported in the corresponding figure legends for all experiments.

REFERENCES

Abbaci M, Barberi-Heyob M, Blondel W, Guillemin F, Didelon J (2008). Advantages and limitations of commonly used methods to assay the molecular permeability of gap junctional intercellular communication. Biotechniques 45, 33–52, 56–62.

Abbaci M, Barberi-Heyob M, Stines JR, Blondel W, Dumas D, Guillemin F, Didelon J (2007). Gap junctional intercellular communication capacity by gap-FRAP technique: a comparative study. Biotechnol J 2, 50–61.

Akoyev V, Takemoto DJ (2007). ZO-1 is required for protein kinase C gamma-driven disassembly of connexin 43. Cell Signal 19, 958–967.

Baker SM, Kim N, Gumpert AM, Segretain D, Falk MM (2008). Acute internalization of gap junctions in vascular endothelial cells in response to inflammatory mediator-induced G-protein coupled receptor activation. FEBS Lett 582, 4039–4046.

Bastide B, Herve JC, Cronier L, Deleze J (1995). Rapid onset and calcium independence of the gap junction uncoupling induced by heptanol in cultured heart cells. Pflugers Arch 429, 386–393.

Bats C, Groc L, Choquet D (2007). The interaction between Stargazin and PSD-95 regulates AMPA receptor surface trafficking. Neuron 53, 719–734.

Bruce AF, Rothery S, Dupont E, Severs NJ (2008). Gap junction remodelling in human heart failure is associated with increased interaction of connexin43 with ZO-1. Cardiovasc Res 77, 757–765.

Clarke TC, Williams OJ, Martin PE, Evans WH (2009). ATP release by cardiac myocytes in a simulated ischaemia model: inhibition by a connexin mimetic and enhancement by an antiarrhythmic peptide. Eur J Pharmacol 605, 9–14.

Contreras JE, Saez JC, Bukauskas FF, Bennett MV (2003). Gating and regulation of connexin 43 (Cx43) hemichannels. Proc Natl Acad Sci USA 100, 11388–11393.

Cotrina ML, Lin JH, Nedergaard M (2008). Adhesive properties of connexin hemichannels. Glia 56, 1791–1798.

Coutinho P, Qiu C, Frank S, Tamber K, Becker D (2003). Dynamic changes in connexin expression correlate with key events in the wound healing process. Cell Biol Int 27, 525–541.

Darrow BJ, Laing JG, Lampe PD, Saffitz JE, Beyer EC (1995). Expression of multiple connexins in cultured neonatal rat ventricular myocytes. Circ Res 76, 381–387.

Desplantez T, Dupont E, Severs NJ, Weingart R (2007). Gap junction channels and cardiac impulse propagation. J Membr Biol 218, 13–28.

Doble BW, Dang X, Ping P, Fandrich RR, Nickel BE, Jin Y, Cattini PA, Kardami E (2004). Phosphorylation of serine 262 in the gap junction protein connexin-43 regulates DNA synthesis in cell-cell contact forming cardiomyocytes. J Cell Sci 117, 507–514.

Ek-Vitorin JF, King TJ, Heyman NS, Lampe PD, Burt JM (2006). Selectivity of connexin 43 channels is regulated through protein kinase C-dependent phosphorylation. Circ Res 98, 1498–1505.

Elias LA, Wang DD, Kriegstein AR (2007). Gap junction adhesion is necessary for radial migration in the neocortex. Nature 448, 901–907.

Fox JE, Lipfert L, Clark EA, Reynolds CC, Austin CD, Brugge JS (1993). On the role of the platelet membrane skeleton in mediating signal transduction. Association of GP IIb-IIIa, pp60c-src, pp62c-yes, and the p21ras GTPase-activating protein with the membrane skeleton. J Biol Chem 268, 25973–25984.

Gaietta G, Deerinck TJ, Adams SR, Bouwer J, Tour O, Laird DW, Sosinsky GE, Tsien RY, Ellisman MH (2002). Multicolor and electron microscopic imaging of connexin trafficking. Science 296, 503–507.

Giepmans BN (2004). Gap junctions and connexin-interacting proteins. Cardiovasc Res 62, 233–245.

Giepmans BN, Moolenaar WH (1998). The gap junction protein connexin43 interacts with the second PDZ domain of the zona occludens-1 protein. Curr Biol 8, 931–934.

Gilleron J, Fiorini C, Carette D, Avondet C, Falk MM, Segretain D, Pointis G (2008). Molecular reorganization of Cx43, ZO-1 and Src complexes during the endocytosis of gap junction plaques in response to a nongenomic carcinogen. J Cell Sci 121, 4069–4078.

Goliger JA, Paul DL (1995). Wounding alters epidermal connexin expression and gap junction-mediated intercellular communication. Mol Biol Cell 6, 1491–1501.

Gonzalez-Mariscal L, Betanzos A, Avila-Flores A (2000). MAGUK proteins: structure and role in the tight junction. Semin Cell Dev Biol 11, 315–324.

Gourdie RG, Green CR, Severs NJ (1991). Gap junction distribution in adult mammalian myocardium revealed by an anti-peptide antibody and laser scanning confocal microscopy. J Cell Sci 99, 41–55.

Green CR, Peters NS, Gourdie RG, Rothery S, Severs NJ (1993). Validation of immunohistochemical quantification in confocal scanning laser microscopy: a comparative assessment of gap junction size with confocal and ultrastructural techniques. J Histochem Cytochem 41, 1339–1349.

Gullberg M, AC Andersson (2010). Visualization and quantification of protein-protein interactions in cells and tissues. Nat Med 7, v–vi.

Guo H, Acevedo P, Parsa FD, Bertram JS (1992). Gap-junctional protein connexin 43 is expressed in dermis and epidermis of human skin: differential modulation by retinoids. J Invest Dermatol 99, 460–467.

Hendrix EM, Mao SJ, Everson W, Larsen WJ (1992). Myometrial connexin 43 trafficking and gap junction assembly at term and in preterm labor. Mol Reprod Dev 33, 27–38.

Hunter AW, Barker RJ, Zhu C, Gourdie RG (2005). Zonula occludens-1 alters connexin43 gap junction size and organization by influencing channel accretion. Mol Biol Cell 16, 5686–5698.

Hunter AW, Gourdie RG (2008). The second PDZ domain of zonula occludens-1 is dispensable for targeting to connexin 43 gap junctions. Cell Commun Adhes 15, 55–63.

Hunter AW, Jourdan J, Gourdie RG (2003). Fusion of GFP to the carboxyl terminus of connexin43 increases gap junction size in HeLa cells. Cell Commun Adhes 10, 211–214.

John SA, Kondo R, Wang SY, Goldhaber JI, Weiss JN (1999). Connexin-43 hemichannels opened by metabolic inhibition. J Biol Chem 274, 236–240.

Jordan K, Solan JL, Dominguez M, Sia M, Hand A, Lampe PD, Laird DW (1999). Trafficking, assembly, and function of a connexin43-green fluorescent protein chimera in live mammalian cells. Mol Biol Cell 10, 2033–2050.

Kaprielian RR et al. (1998). Downregulation of immunodetectable connexin43 and decreased gap junction size in the pathogenesis of chronic hibernation in the human left ventricle [see comments]. Circulation 97, 651–660.

Kieken F, Mutsaers N, Dolmatova E, Virgil K, Wit AL, Kellezi A, Hirst-Jensen BJ, Duffy HS, Sorgen PL (2009). Structural and molecular mechanisms of gap junction remodeling in epicardial border zone myocytes following myocardial infarction. Circ Res 104, 1103–1112.

Koval M (2006). Pathways and control of connexin oligomerization. Trends Cell Biol 16, 159–166.

Kretz M, Maass K, Willecke K (2004). Expression and function of connexins in the epidermis, analyzed with transgenic mouse mutants. Eur J Cell Biol 83, 647–654.

Kreuzberg MM, Willecke K, Bukauskas FF (2006). Connexin-mediated cardiac impulse propagation: connexin 30.2 slows atrioventricular conduction in mouse heart. Trends Cardiovasc Med 16, 266–272.

Laird DW (1996). The life cycle of a connexin: gap junction formation, removal, and degradation. J Bioenerg Biomembr 28, 311–318.

Laird DW (2006). Life cycle of connexins in health and disease. Biochem J 394, 527–543.

Laird DW, Puranam KL, Revel JP (1991). Turnover and phosphorylation dynamics of connexin43 gap junction protein in cultured cardiac myocytes. Biochem J 273, 67–72.

Lampe PD, Lau AF (2004). The effects of connexin phosphorylation on gap junctional communication. Int J Biochem Cell Biol 36, 1171–1186.

Lauf U, Giepmans BN, Lopez P, Braconnot S, Chen SC, Falk MM (2002). Dynamic trafficking and delivery of connexons to the plasma membrane and accretion to gap junctions in living cells. Proc Natl Acad Sci USA 99, 10446–10451.

Li H, Liu TF, Lazrak A, Peracchia C, Goldberg GS, Lampe PD, Johnson RG (1996). Properties and regulation of gap junctional hemichannels in the plasma membranes of cultured cells. J Cell Biol 134, 1019–1030.

Lin JH et al. (2002). Connexin 43 enhances the adhesivity and mediates the invasion of malignant glioma cells. J Neurosci 22, 4302–4311.

Maass K, Shibayama J, Chase SE, Willecke K, Delmar M (2007). C-terminal truncation of connexin43 changes number, size, and localization of cardiac gap junction plaques. Circ Res 101, 1283–1291.

Martin PE, Evans WH (2004). Incorporation of connexins into plasma membranes and gap junctions. Cardiovasc Res 62, 378–387.

Matsushita T, Oyamada M, Fujimoto K, Yasuda Y, Masuda S, Wada Y, Oka T, Takamatsu T (1999). Remodeling of cell-cell and cell-extracellular matrix interactions at the border zone of rat myocardial infarcts. Circ Res 85, 1046–1055.

Miquerol L, Dupays L, Theveniau-Ruissy M, Alcolea S, Jarry-Guichard T, Abran P, Gros D (2003). Gap junctional connexins in the developing mouse cardiac conduction system. Novartis Found Symp 250, 80–98; discussion 98–109, 276–109.

Musil LS, Goodenough DA (1991). Biochemical analysis of connexin43 intracellular transport, phosphorylation, and assembly into gap junctional plaques. J Cell Biol 115, 1357–1374.

Noorman M, Van Der Heyden MA, van Veen TA, Cox MG, Hauer RN, de Bakker JM, van Rijen HV (2009). Cardiac cell-cell junctions in health and disease: electrical versus mechanical coupling. J Mol Cell Cardiol 47, 23–31.

O'Quinn MP, Palatinus JA, Harris BS, Hewett KW, Gourdie RG (2011). A peptide mimetic of the connexin43 carboxyl terminus reduces gap junction remodeling and induced arrhythmia following ventricular injury. Circ Res 108, 704–715.

Oyamada M, Oyamada Y, Takamatsu T (2005). Regulation of connexin expression. Biochim Biophys Acta 1719, 6–23.

Paulson AF, Lampe PD, Meyer RA, TenBroek E, Atkinson MM, Walseth TF, Johnson RG (2000). Cyclic AMP and LDL trigger a rapid enhancement in gap junction assembly through a stimulation of connexin trafficking. J Cell Sci 113, 3037–3049.

Retamal MA, Schalper KA, Shoji KF, Bennett MV, Saez JC (2007). Opening of connexin 43 hemichannels is increased by lowering intracellular redox potential. Proc Natl Acad Sci USA 104, 8322–8327.

Richards TS, Dunn CA, Carter WG, Usui ML, Olerud JE, Lampe PD (2004). Protein kinase C spatially and temporally regulates gap junctional communication during human wound repair via phosphorylation of connexin43 on serine368. J Cell Biol 167, 555–562.

Ryeom SW, Paul D, Goodenough DA (2000). Truncation mutants of the tight junction protein ZO-1 disrupt corneal epithelial cell morphology. Mol Biol Cell 11, 1687–1696.

Saez JC, Berthoud VM, Branes MC, Martinez AD, Beyer EC (2003). Plasma membrane channels formed by connexins: their regulation and functions. Physiol Rev 83, 1359–1400.

Saez JC, Retamal MA, Basilio D, Bukauskas FF, Bennett MV (2005). Connexin-based gap junction hemichannels: gating mechanisms. Biochim Biophys Acta 1711, 215–224.

Saffitz JE, Laing JG, Yamada KA (2000). Connexin expression and turnover: implications for cardiac excitability. Circ Res 86, 723–728.

Salmon ED, Leslie RJ, Saxton WM, Karow ML, McIntosh JR (1984). Spindle microtubule dynamics in sea urchin embryos: analysis using a fluorescein-labeled tubulin and measurements of fluorescence redistribution after laser photobleaching. J Cell Biol 99, 2165–2174.

Severs NJ, Bruce AF, Dupont E, Rothery S (2008). Remodelling of gap junctions and connexin expression in diseased myocardium. Cardiovasc Res 80, 9–19.

Shaw RM, Fay AJ, Puthenveedu MA, von Zastrow M, Jan YN, Jan LY (2007). Microtubule plus-end-tracking proteins target gap junctions directly from the cell interior to adherens junctions. Cell 128, 547–560.

Shintani-Ishida K, Uemura K, Yoshida K (2007). Hemichannels in cardiomyocytes open transiently during ischemia and contribute to reperfusion injury following brief ischemia. Am J Physiol Heart Circ Physiol 293, H1714–1720.

Singh D, Solan JL, Taffet SM, Javier R, Lampe PD (2005). Connexin 43 interacts with zona occludens-1 and -2 proteins in a cell cycle stage-specific manner. J Biol Chem 280, 30416–30421.

Smith JH, Green CR, Peters NS, Rothery S, Severs NJ (1991). Altered patterns of gap junction distribution in ischemic heart disease. An immunohistochemical study of human myocardium using laser scanning confocal microscopy. Am J Pathol 139, 801–821.

Solan JL, Fry MD, TenBroek EM, Lampe PD (2003). Connexin43 phosphorylation at S368 is acute during S and G2/M and in response to protein kinase C activation. J Cell Sci 116, 2203–2211.

Solan JL, Lampe PD (2009). Connexin43 phosphorylation: structural changes and biological effects. Biochem J 419, 261–272.

Thomas T, Jordan K, Simek J, Shao Q, Jedeszko C, Walton P, Laird DW (2005). Mechanisms of Cx43 and Cx26 transport to the plasma membrane and gap junction regeneration. J Cell Sci 118, 4451–4462.

Tong D, Li TY, Naus KE, Bai D, Kidder GM (2007). In vivo analysis of undocked connexin43 gap junction hemichannels in ovarian granulosa cells. J Cell Sci 120, 4016–4024.

Toyofuku T, Yabuki M, Otsu K, Kuzuya T, Hori M, Tada M (1998). Direct association of the gap junction protein connexin-43 with ZO-1 in cardiac myocytes. J Biol Chem 273, 12725–12731.

van Veen AA, van Rijen HV, Opthof T (2001). Cardiac gap junction channels: modulation of expression and channel properties. Cardiovasc Res 51, 217–229.

VanSlyke JK, Musil LS (2005). Cytosolic stress reduces degradation of connexin43 internalized from the cell surface and enhances gap junction formation and function. Mol Biol Cell 16, 5247–5257.

Yum SW, Zhang J, Valiunas V, Kanaporis G, Brink PR, White TW, Scherer SS (2007). Human connexin26 and connexin30 form functional heteromeric and heterotypic channels. Am J Physiol Cell Physiol 293, C1032–1048.

Zhu C, Barker RJ, Hunter AW, Zhang Y, Jourdan J, Gourdie RG (2005). Quantitative analysis of ZO-1 colocalization with Cx43 gap junction plaques in cultures of rat neonatal cardiomyocytes. Microsc Microanal 11, 244–248.